Journal of Physics and Chemistry of Solids 118 (2018) 137–143

Contents lists available at ScienceDirect

Journal of Physics and Chemistry of Solids

journal homepage: www.elsevier.com/locate/jpcs

# High porous bio-nanocarbons prepared by carbonization and NaOH activation of polysaccharides for electrode material of EDLC

Kenji Takeuchi [a], Masatsugu Fujishige [a], Nobuaki Ishida [a], Yoshihiro Kunieda [a], Yosuke Kato [a], Yusuke Tanaka [a], Toshiyuki Ochi [b], Hisashi Shirotori [c], Yuji Uzuhashi [b], Suguru Ito [a], Kyo-ichi Oshida [d], Morinobu Endo [a,*]

[a] Institute of Carbon Science and Technology, Shinshu University, 4-17-1 Wakasato, Nagano-city, Nagano, 380-8553, Japan
[b] Ina Food Industry Co., Ltd., Nishi-haruchika, Ina-city, Nagano, 399-4497, Japan
[c] Rubycon Corporation, 1938-1 Nishi-Minowa, Ina-city, Nagano, 399-4593, Japan
[d] Nagano National College of Technology, 716 Tokuma, Nagano, 380-8550, Japan

ARTICLE INFO

*Keywords:*
Polysaccharides
Nanocarbon
NaOH
Activated carbon
EDLC

ABSTRACT

Carbonization and post-activation of polysaccharides (utilized as food residue) created new bio-nanocarbons for the electrode of electric double layer capacitors (EDLC). Large specific capacitance (46.1 F/g, 26.4 F/cm$^3$) and high rate performance was confirmed under optimized conditions of carbonization temperature (600 °C) and supplied amount of sodium hydroxide in NaOH-activation process (250 wt %). The capacitance and rate performance were larger than the reported values, 42.9 F/g, 19.7 F/cm$^3$ of currently used activated carbon MSP-20. The feature that NaOH is usable as the activation agent, instead of KOH, is advantageous for reducing the cost of EDLC.

## 1. Introduction

Problems of energy crisis, environmental pollution and global warming are needed to be solved by facile, eco-friendly and cost-effective technologies [1]. Biomass is one of candidates as energy source in such new technology [2,3]. With increasing unused resources of agricultural, forest and fishery products, its effective utilization is becoming important. Polysaccharides, utilized as food, are produced from natural plants such as seaweeds and grains. Because food residue originated from polysaccharides is eco-friendly, cheap and available in large quantity, it has a bright prospect as feedstock of bio-nanocarbons. Polysaccharides possess considerable amounts of pores. Such pores remain after carbonization so that appropriate activation creates functional bio-nanocarbons. In addition, the fact that polysaccharides contain oxygen (ca. 30 at. %) in their structure is also favorable for producing highly porous carbonaceous materials through pyrolysis and post-activation.

A lot of investigation on the pyrolysis of biomass materials has been reported [4–13]. For example, hydrothermal carbonization and post-activation of lignocellulosic feedstock brought about carbonaceous adsorbent with high surface area of 2511 m$^2$/g applicable for selective $CO_2$-adsorption [4]. On the other hand, a variety of carbon materials is applicable for EDLC (electric double layer capacitors) electrode [14–18]. Because EDLC accumulates electric charge through adsorption of ions, high rate charging and discharging is possible and discharging density is very large. Since it includes carbon for anode and cathode, the performance depends largely on the structure of carbon. Because energy density of EDLC is lower than that of LIB (lithium ion battery), improvement of charge capacity and cost-effective process is required for practical applications of EDLC. Activated charcoals, derived from palm trees, are generally now in common use for the electrode material of EDLC. Further, it includes high-cost activation with potassium hydroxide (KOH). The present paper investigated carbonization behavior of polysaccharides for the application to EDLC electrode. It involves the effect of carbonization temperatures and activation with different amounts of sodium hydroxide (NaOH) on properties such as particle size and shape, carbon properties, pore size distribution, surface area, and electrochemical performances.

## 2. Experimental

Fig. S1 shows schematic representation of the present study aiming at clarifying electrochemical behavior of bio-nanocarbons prepared by

* Corresponding author.
*E-mail address:* endo@endomoribu.shinshu-u.ac.jp (M. Endo).

https://doi.org/10.1016/j.jpcs.2018.02.050
Received 18 January 2018; Received in revised form 21 February 2018; Accepted 22 February 2018
Available online 28 February 2018

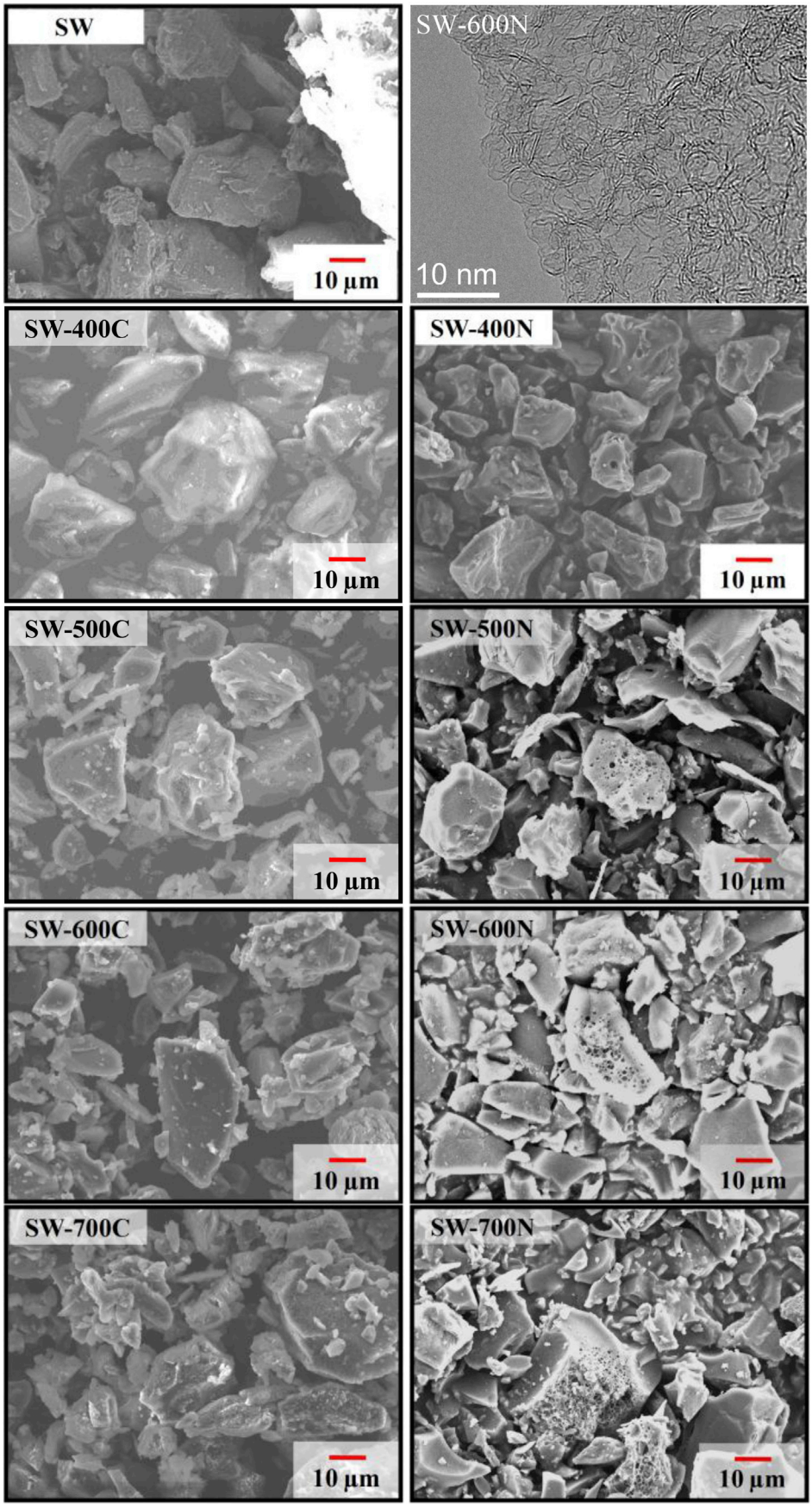


**Fig. 1.** FE-SEM images of original polysaccharides (SW), carbonized nanocarbons (SW-400C, 500C, 600C, 700C), activated nanocarbons (SW-600N, 500N, 600N, 700N) and TEM image of SW-600N.

carbonization and NaOH activation of polysaccharides for the application to the electrode of EDLC. Because carbonization process involves pore formation and crystal growth, proper selection of carbonization temperature is important for effective activation of the resultant carbon materials. Fig. S2 is TG-DTA of polysaccharides (utilized as food residue, glucan with molecular weight of $2.5 \times 10^6$, Ina Food Industry Co., Ltd., XZ-718; SW) in argon atmosphere. It showed steep weight decrease due to exothermal reaction below 500 °C and then they became stable above 500 °C. Thus, the present investigation carried out carbonization by keeping polysaccharides in an electric furnace kept at 400 °C, 500 °C, 600 °C and 700 °C for 1 h in argon atmosphere (hereafter these samples are designated by the sample ID as follows: SW-400C, SW-500C, SW-600C and SW-700C).

The activation of carbonized samples was carried out by adding NaOH (250 wt %) as activation agent and the mixture was heat-treated at 720 °C for 1 h in argon atmosphere (hereafter these samples are designated by the sample ID as follows: SW-400N, SW-500N, SW-600N and SW-700N). For comparison, KOH was used instead of NaOH in separate experiments. The morphology of the samples was observed by scanning electron microscope (SEM, JSM-7000F-JEOL) and high-resolution transmission electron microscopy (TEM, 2100F-JEOL) with Cs corrector. The Raman spectra were measured by inVia Raman microscope (Renishaw) using a light with $\lambda = 532$ nm. The nitrogen-adsorption isotherms of BC and AC samples at 77 K were observed by the gas adsorption analyzers (ASAP 2020-Micromeritics). The BET surface area and pore volume were determined from the adsorption isotherms. The calculation of the pore volume was performed based on the method of the density functional theory (DFT) [19] and Fast Fourier Transform (FFT). The XPS measurement of the samples was carried out by Kratos AXIS-ULTRA.

The bio-nanocarbon thus prepared was mixed with PTFE (5 wt %). The mixed sample (20 mg) was then poured in a metal mold with diameter of 1 cm. By applying pressure of 9.8 kN on it, a disk electrode was prepared. Two pieces of disk electrode were prepared. Their weight and thickness were measured. A separator was set between them and interposed by collecting electrodes. It was then fixed with PTFE plates. To avoid water contamination, organic electrolyte ($Et_4NBF_4$/PC) was poured in a beaker in a glove box under argon atmosphere, and then the cell was left in the electrolyte under vacuum for 24 h to penetrate electrolyte in the electrodes. The capacitance of the EDLC was calculated from the charge and discharge curves.

## 3. Results and discussions

Fig. 1 shows FE-SEM images of pristine, carbonized and activated samples. The particle size of pristine polysaccharides is approximately 50 μm. It became 20–30 μm after carbonization. This shrinkage is due to release of heteroatoms such as oxygen and hydrogen during carbonization. Among carbonized samples, SW-400C (heat-treated polysaccharides sample at 400 °C) has rotundity shape in contrast to angular shape of SW-500C, SW-600C and SW-700C. This observation suggests that the carbonization occurs at temperatures higher than 500 °C and heterogeneous texture develops along with development of carbon network. The particle size did not change during activation treatment. The number of fine deposits, observed for carbonized sample, decreased after activation. Two possible explanations are as follows: The deposits were removed by chemical attack of NaOH during activation, or development of carbon network during heat-treatment yielded flat and smooth surface.

Fig. 2 shows Raman spectra of carbonized and activated samples. Each spectrum is composed of D band at around 1360 $cm^{-1}$ and G band at around 1580 $cm^{-1}$ as is usually observed for carbon materials [20]. The R-values (intensity ratio of D to G bands) and FWHM of G-band are summarized in Table S1. For carbonized samples, R-value increases with increasing carbonization temperature. The FWHM of G-band decreases with increasing carbonization temperature. They are indications of the feature that the carbon network develops with increasing heat-treatment temperature, while considerable amounts of defects were introduced due to releasing of heteroatoms. Comparison of the spectra of carbonized and activated samples heat-treated at the same temperature indicates that the activated sample has larger R-values. This is due to increase of defects during activation process.

Table 1 summarizes chemical compositions of pristine, carbonized and activated samples, estimated by XPS. Pristine polysaccharides consist of carbon, oxygen and sodium. The carbon content decreases monotonically with increasing carbonization temperature above 500 °C, in contrast to the increase of sodium content. This observation shows that removal of carbon takes place during heat-treatment and sodium remains in the residue; the release of molecules containing carbon and oxygen with low boiling point takes place during heat-treatment. The oxygen content increased with increasing carbonization temperature above 600 °C. Because the release of $CH_4$ starts to take place at around 600 °C, the carbon content decreased with temperature between 500 and 700 °C; as a result, the oxygen content increased with temperature in this region.

**Table 1**
Chemical composition of pristine polysaccharides (SW), carbonized and activated nanocarbons derived from polysaccharides estimated by XPS.

| Sample I. D. | C [at. %] | O [at. %] | Na [at. %] |
|---|---|---|---|
| SW | 64.7 | 64.7 | 1.1 |
| SW-400C | 62.9 | 62.9 | 9.5 |
| SW-500C | 53.1 | 53.1 | 13.8 |
| SW-600C | 45.2 | 45.2 | 17.2 |
| SW-700C | 37.1 | 37.1 | 22.3 |
| SW-400N | 93.0 | 7.0 | 0 |
| SW-500N | 93.5 | 6.5 | 0 |
| SW-600N | 93.1 | 6.9 | 0 |
| SW-700N | 90.0 | 10.0 | 0 |

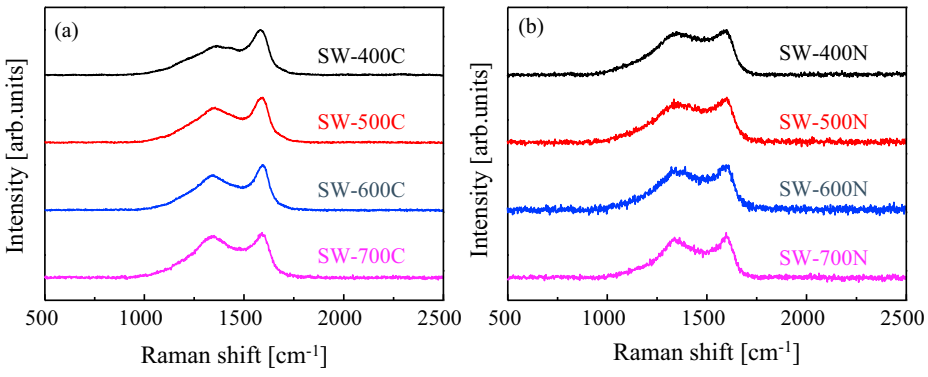


**Fig. 2.** Raman spectra of (a) carbonized and (b) activated nanocarbons derived from polysaccharides.

Contrary to the carbonized samples, activated samples do not contain sodium. Because it was washed with water after activation, sodium carbonate was eliminated from the sample. It is noteworthy that the carbon content exceeds 90 at. % for activated samples. This is because molecules containing oxygen, with low boiling point, released during activation process.

Fig. S3 shows the nitrogen-adsorption isotherms of activated samples at 77 K. All the samples show steep increase of adsorbed volume in the lower pressure region. Therefore, activated sample is porous material involving micro-pores. The adsorbed amount decreases with increasing carbonization temperature. The development of carbon network planes reduces the number of active site effective for the NaOH activation.

Fig. 3 is the pore-size distribution obtained by TEM image and image processing (FFT) combined method [21], which is very similar to that obtained by DFT (Fig. S4). Table 2 summarizes their specific surface area and pore size distributions (DFT method). The pore size distributions become narrow and the mean value of pore size tends to be small with increasing carbonization temperature. The carbon network develops with increasing carbonization temperature and therefore extraction of carbon by NaOH tends to be difficult in the activation process. The specific volume of activated samples decreases with increasing carbonization temperature from 500 °C to 700 °C as is seen in Table 2. This is due to decrease of activation efficiency with increasing carbonization temperature. Variation of the amount of the micro-pore volume with carbonization temperature shows similar trend with that of specific surface area. It suggests that the micro-pore volume is important for nitrogen adsorption capacity. Thus, the pore of bio-nanocarbons, derived from polysaccharides, consists of mainly micro-pore and minor component (10–20%) of meso-pore.

**Table 2**
Specific surface area and pore size distribution of activated nanocarbons derived from polysaccharides.

| Sample I. D. | Specific surface area [$m^2/g$] | Pore volume [$cm^3/g$] | Micro pore volume [$cm^3/g$] | Meso pore volume [$cm^3/g$] | Ratio of Meso pore volume [%] |
|---|---|---|---|---|---|
| SW-400N | 2498.6 | 1.08 | 0.82 | 0.26 | 24.1 |
| SW-500N | 2551.7 | 1.00 | 0.86 | 0.14 | 14.0 |
| SW-600N | 2294.3 | 0.84 | 0.76 | 0.08 | 9.6 |
| SW-700N | 1498.9 | 0.50 | 0.48 | 0.02 | 4.0 |

Fig. 4a shows charge-discharge curves under constant current of disk electrode with different carbonization temperature, where (a) represent specific capacity in F/g and (b) in $F/cm^3$. The data of MSP-20 (Kansai Coke and Chemicals Company, Ltd.: currently used for commercial EDLC) is also shown for comparison. Table 3a summarizes the effect of carbonization temperature on the maximum capacity, electrode density and rate performance. The specific weight capacity (F/g) decreases with increasing carbonization temperature due to decrease of specific surface area (decrease of adsorption site of ions). The specific volume capacity ($F/cm^3$) of SW-600N was the largest among 5 samples tested. The specific volume capacity is the product of specific weight capacity and electrode density. SW-600N has relatively large values both in weight capacity and in electrode density, in addition to high rate performance. The rate

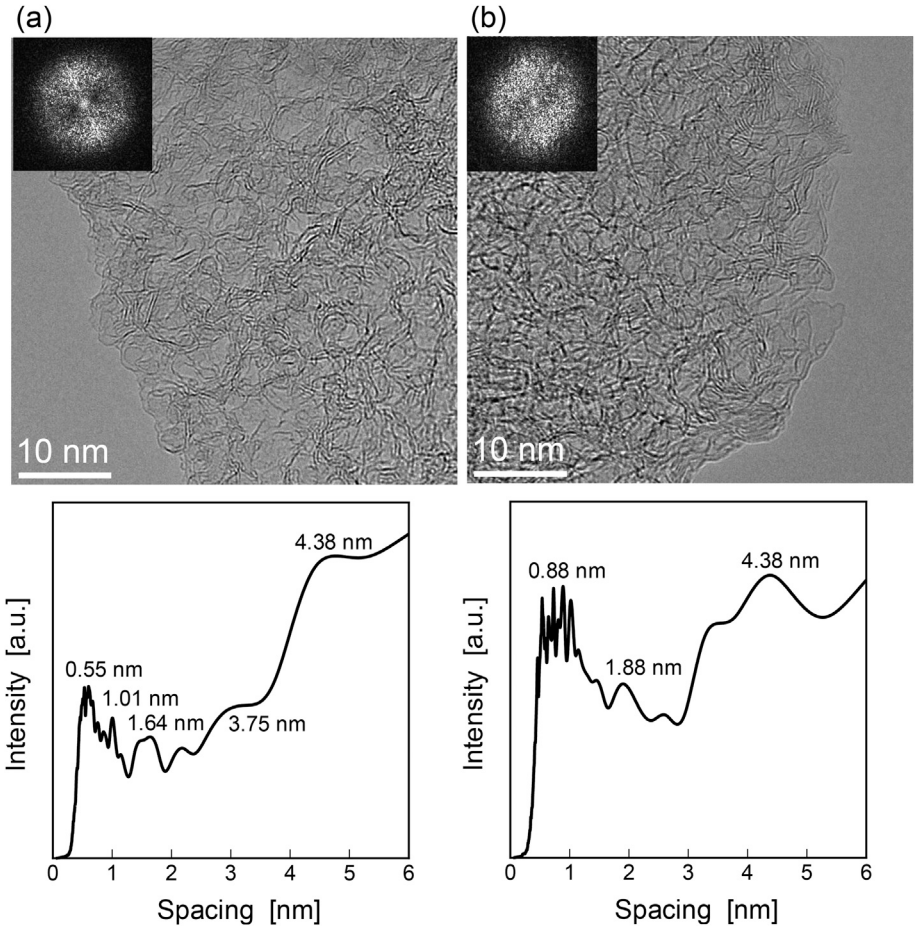


**Fig. 3.** TEM images of (a) activated nanocarbon (SW-600N) and (b) commercially available MSP-20 and pore analysis by image processing (FFT).

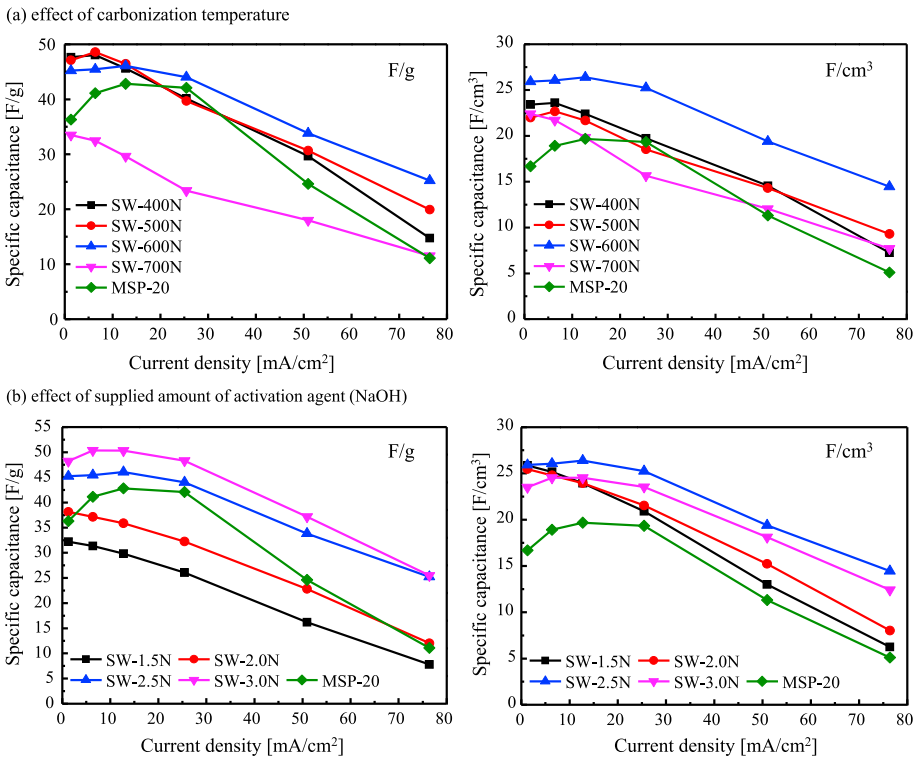


**Fig. 4.** Capacity of activated nanocarbons and commercially available MSP-20 plotted as a function of current density: (a) effect of carbonization temperature, (b) effect of supplied amount of activation agent (NaOH).

**Table 3**
Maximum capacity, electrode density and rate performance of activated nanocarbons derived from polysaccharides and commercial MSP-20: (a) effect of carbonization temperature, (b) effect of supplied amount of activation agent (NaOH).

(a) effect of carbonization temperature

| Sample I. D. | $C_{Max}$ [F/g] | $C_{Max}$ [F/cm$^3$] | Electrode density [g/cm$^3$] | Rate Performance (volume capacity) | | | | |
|---|---|---|---|---|---|---|---|---|
| | | | | 5mA/1 mA | 10mA/1 mA | 20mA/1 mA | 40mA/1 mA | 60mA/1 mA |
| SW-400N | 48.0 | 23.6 | 0.491 | 100.8 | 95.7 | 84.2 | 62.2 | 30.9 |
| SW-500N | 48.6 | 22.7 | 0.466 | 103.1 | 98.6 | 84.3 | 65.1 | 42.3 |
| SW-600N | 46.1 | 26.4 | 0.573 | 100.5 | 101.9 | 97.4 | 74.8 | 55.8 |
| SW-700N | 33.5 | 22.4 | 0.669 | 96.9 | 88.5 | 69.8 | 53.7 | 34.4 |
| MSP-20 | 42.9 | 19.7 | 0.460 | 113.3 | 118.0 | 115.4 | 67.8 | 30.5 |

(b) effect of supplied amount of activation agent (NaOH)

| Activation agent | Sample I. D. | $C_{Max}$ [F/g] | $C_{Max}$ [F/cm$^3$] | Electrode density [g/cm$^3$] | Rate Performance (volume capacity) | | | | |
|---|---|---|---|---|---|---|---|---|---|
| | | | | | 5mA/1 mA | 10mA/1 mA | 20mA/1 mA | 40mA/1 mA | 60mA/1 mA |
| NaOH | SW-1.5N | 32.1 | 25.9 | 0.803 | 97.3 | 86.8 | 68.4 | 46.6 | 24.2 |
| | SW-2.0N | 36.7 | 25.8 | 0.668 | 97.4 | 94.0 | 84.5 | 59.8 | 31.5 |
| | SW-2.5N | 46.1 | 26.4 | 0.573 | 100.5 | 101.9 | 97.4 | 74.8 | 55.8 |
| | SW-3.0N | 50.3 | 24.5 | 0.487 | 104.4 | 104.4 | 100.2 | 77.1 | 52.8 |
| KOH | SW-1.5K | 26.2 | 21.5 | 0.820 | 72.7 | 57.3 | 43.3 | – | – |
| | SW-2.0K | 38.1 | 25.5 | 0.668 | 97.1 | 92.5 | 79.1 | 65.8 | 49.8 |
| | SW-2.5K | 34.9 | 24.9 | 0.712 | 64.8 | 49.8 | 46.8 | – | – |
| – | MSP-20 | 42.9 | 19.7 | 0.460 | 113.3 | 118.0 | 115.4 | 67.8 | 30.5 |

performance usually depends on the electric conductivity and ionic mobility. The increase of carbonization temperature is advantageous for electric conductivity but disadvantageous for ionic mobility due to decrease of meso-pores. Thus, above results indicate that the optimum carbonization temperature is 600 °C. It is important to mention that SW-600N has larger capacity and higher rate performance than MSP-20, which usually used for EDLC electrode. This observation shows possibility of the present bio-nanocarbon for the application to EDLC electrode.

Fig. 4b shows the effect of supplied amount of NaOH in the activation process on the charge-discharge performance under constant current, where (a) represent capacity in F/g and (b) in F/cm$^3$. Fig. S5 shows the CV curves of SW samples for different scan rate. From these results, the maximum capacity, electrode density and rate performance were estimated and listed in Table 3b, where the data for KOH activated bio-nanocarbon is also shown for comparison. The weight capacity increased with increasing supplied amount of NaOH. The pore size distribution of these SW samples showed that the specific surface area

increased with increasing supplied amount of NaOH. On the other hand, such a simple relation is not observed between volume capacity and supplied amount of NaOH. The volume capacity of SW-3.0N is the minimum among 4 samples. Although the increase of pore volume is advantageous for ion adsorption, it induces the decrease of electrode density at the same time. Among SW-1.5N, SW-2.0N and SW-2.5N, SW-2.5N has the largest specific surface area and meso-pore volume in addition to fairly large electrode density resulting in high rate performance. Thus, the optimum supplied amount of NaOH to carbonized material is 250 wt %. Currently, KOH is generally used for the activation of carbon materials [22–28]. Contrary to such general trend, the present investigation claimed that NaOH is usable for the activating carbonized polysaccharides. Its electrochemical performance is comparable to that of KOH activated samples. This finding opens a new eco-friendly and cost-effective route for preparing EDLC electrode.

It is reported that carbon activation with KOH proceeds according to equation (1) [29,30].

$$6KOH + 2C \rightarrow 2K + 3H_2 + 2K_2CO_3 \quad (1)$$

Similarly, the reaction scheme of the carbon activation with NaOH can be expressed in the same manner as equation (2) [31].

$$6NaOH + 2C \rightarrow 2Na + 3H_2 + 2Na_2CO_3 \quad (2)$$

Comparative study of KOH and NaOH activation of multi-walled carbon nanotubes (MWCNTs) showed that NaOH is only effective with disordered MWCNTs whereas KOH is effective whatever the structural order [32]. The differences found between KOH and NaOH are related with an additional intercalation step of metallic K or Na. Metallic K can intercalates all materials in contrast with Na which can only intercalate disorganized carbons. The metal intercalation causes the separation of carbon layers, which generates micropores or even new high energy sites for the activation reaction. The carbons derived from polysaccharides have disorganized structure as is seen in the Raman spectra (Fig. 2a). Therefore, NaOH activation was also effective for micropore formation and hence EDLC performance.

## 4. Conclusions

The present study proposed highly functional bio-nanocarbons prepared through carbonization of polysaccharides and post-activation by NaOH as the EDLC electrode. By optimizing the carbonization and activation conditions (600 °C and 250 wt % of supplied amount of NaOH), large capacity (46.1 F/g, 26.4 F/cm$^3$) and high rate performances (74%: volume capacity ratio between 5mA/1 mA and 40mA/1 mA) have been observed. These values are superior to 42.9 F/g, 19.7 F/cm$^3$ and 59%, respectively, reported for currently used commercial electrode (activated carbon, MSP-20). Capacity and rate performances are generally in a relation of trade-off. Therefore, commercial EDLC electrodes are classified to two types: large capacity type and rapid charging and discharging type (high rate performances). On the other hand, the present bio-nanocarbon has both large capacity and high rate performances, possible to use a variety of applications. In addition, NaOH can be used in the activation process, instead of KOH. This feature is advantageous to reduce the cost of EDLC.

## Acknowledgements

This research was supported by grants from the Project of the NARO Bio-oriented Technology Research Advancement Institution (Integration research for agriculture and interdisciplinary fields), Ministry of Agriculture, Forestry and Fisheries of Japan. Authors thank Dr. Noboru Akuzawa of Shinshu University for his kind suggestions and discussions.

## Appendix A. Supplementary data

Supplementary data related to this article can be found at https://doi.org/10.1016/j.jpcs.2018.02.050.

## References

[1] W-J. Liu, H. Jiang, H.-Q. Yu, Development of biochar-based functional materials: Toward a Sustainable platform carbon material, Chem. Rev. 115 (2015) 12251–12285.
[2] D.M. Alonso, S.G. Wettstein, J.A. Dumesic, Bimetallic catalysts for upgrading of biomass to fuels and chemicals, Chem. Soc. Rev. 41 (2012) 8075–8098.
[3] N. Linares, A.M. Silvestre-Albero, E. Serrano, J. Silvestre-Albero, J. Garcia-Martinez, Mesoporous materials for clean energy technologies, Chem. Rev. Soc. 43 (2014) 7681–7717.
[4] G.K. Parshetti, S. Chowdhury, R. Balasubramanian, Biomass derived low-cot microporous adsorbents for efficient $CO_2$ capture, Fuel 148 (2015) 246–254.
[5] A. Sadaka, H. Liechty, M. Pelkki, M. Blazier, Pyrolysis and combustion kinetics of raw and carbonized cottonwood and switchgrass agroforests, BioResources 10 (2015) 4498–4518.
[6] M. Maketa, V. Benavente, A. Fallana, Hydrothermal carbonization of lignocellulosic biomass: effect of process conditions on hydrochar properties, Appl. Energy 155 (2015) 576–584.
[7] K. Yang, Q. Gao, Y. Tian, W. Qian, L. Zhu, C. Yang, Biomass-derived porous carbon with micropores and small mesopores for high-performance lithium-sulfur batteries, Chem. Eur J. 22 (2016) 3239–3244.
[8] E. Sermyagina, J. Saari, J. Kaikko, E. Vakkilainen, Hydrothermal carbonization of coniferous biomass: effect of process parameters on mass and energy yields, J. Anal. Appl. Pyrolysis 113 (2015) 551–556.
[9] A.M. Smith, S. Singh, A.B. Ross, Fate of inorganic materials during hydrothermal carbonization of biomass: influence of feedstock on combustion behavior of hydrochar, Fuel 169 (2016) 135–145.
[10] H.M. Coromina, D.A. Walsh, R. Mokaya, Biomass-derived activated carbon with simultaneously enhanced CO2 uptake for both pre and post combustion capture applications, J. Mater. Chem. A 4 (2016) 280–289.
[11] A. Jain, R. Balasubramanian, M.P. Srinvasan, Hydrothermal conversion of biomass waste to activated carbon with high porosity: a review, Chem. Eng. J. 283 (2016) 789–805.
[12] P. Han, B. Yang, Z. Qiu, Y. You, J. Jiang, J. Liu, J. Xu, H. Fan, C. Zhu, Air-expansion induced hierarchically porous carbonaceous aerogels from biomass materials with superior lithium storage properties, RSC Adv. 6 (2016) 7591–7598.
[13] M. Wang, C. Wang, M. Chen, Y. Wang, Z. Shi, X. Du, T. Li, Z. Hu, Preparation of high-performance activated carbons for electric double layer capacitors by KOH activation of mesophase pitches, N. Carbon Mater. 25 (4) (2010) 285–290.
[14] Y. Kim, C. Yang, K. Park, K. Kaneko, Y. Ahm, M. . Noguchi, T. Fujino, S. Oyama, M. Endo, Edge-Enriched, porous carbon-based, high energy density supercapacitors for hybrid electric vehicles, ChemSusChem 5 (2012) 535–541.
[15] I.Y. Jang, H. Ogata, K. Park, S.H. Lee, J.S. Park, Y.C. Jung, Y.J. Kim, Y.A. Kim, M. Endo, Exposed edge planes of cup-stacked carbon nanotubes for an electrochemical capacitor, J. Phys. Chem. Lett. 1 (2010) 2099–2103.
[16] Y.J. Kim, I.Y. Jang, K.C. Park, Y.C. Jung, T. Oka, S. Iinou, Y. Komori, T. Kozutsumi, T. Hashiba, Y.A. Kim, M. Endo, High-capacitance supercapacitors using nitrogen-decorated porous carbon derived from novolac resin containing peptide linkage, Electrochim. Acta 55 (2010) 5624–5628.
[17] Y.J. Kim, Y. Abe, T. Yanaglura, K.C. Park, M. Shimizu, T. Iwazaki, S. Nakagawa, M. Endo, M.S. Dresselhaus, Easy preparation of nitrogen-enriched carbon materials from peptides of silk fibroins and their use to produce a high volumetric energy density in supercapacitors, Carbon 45 (2007) 2116–2125.
[18] C. Portet, G. Yushin, Y. Gogotsi, Electrochemical performance of carbon onions, nanodiamonds, carbon black and multiwalled nanotubes in electrical double layer capacitors, Carbon 45 (2007) 2511–2518.
[19] J.P. Olivier, Improving the models used for calculating the size distriburion of micropore volume of activated carbons from adsorption data, Carbon 36 (1998) 1469–1472.
[20] M. Sevilla, A.B. Fuertes, R. Mokaya, High density hydrogen storage in superactivated carbons from hydrothermally carbonized renewable organic materials, Energy Environ. Sci. 4 (2011) 1400–1410.
[21] K. Oshida, K. Kogiso, K. Matsubayashi, S. Kobayashi, M. Endo, M.S. Dresselhaus, G. Dresselhaus, Analysis of pore structure of activated carbon fibers using high resolution transmission electron microscopy and image processing, J. Mater. Res. 10 (10) (1995) 2507–2517.
[22] X. Li, C. Han, X. Chen, C. Shi, Preparation and performance of straw based activated carbon for supercapacitor in non-aqueous electrolytes, Microporous Mesoporous Mater. 131 (2010) 303–309.
[23] M. Armandi, B. Bonelli, F. Geobaldo, E. Garrone, Nanoporous carbon materials obtained by sucrose carbonization in the presence of KOH, Microporous Mesoporous Mater. 132 (2010) 414–420.
[24] M. Sevilla, A.B. Fuertes, R. Mokaya, High density hydrogen storage in superactivated carbons from hydrothermally carbonized renewable organic materials, Energy Environ. Sci. 4 (2011) 1400–1410.
[25] J. Wang, S. Kaskel, KOH activation of carbon based materialsfor energy storage, J. Mater. Chem. 22 (2012) 23710–23725.

[26] H. Wei, S. Deng, B. Hu, Z. Chen, B. Wang, J. Huang, G. Yu, Granular bamboo-derived activated carbon for high CO2 adsorption: the dominant role of narrow micropores, ChemSusChem 5 (2012) 2354–2360.
[27] M. Li, C. Liu, H. Cao, H. Zhao, Y. Zhang, Z. Fan, KOH self-templating synthesis of three-dimensional hierarchical porous carbon materials for high performance supercapacitors, J. Mater. Chem. A 2 (2014) 14844–14851.
[28] W. Qian, F. Sun, Y. Xu, L. Qiu, C. Liu, S. Wang, F. Yan, Human hair-derived carbon flakes for electrochemical supercapacitors, Energy Environ. Sci. 7 (2014) 379–386.
[29] T. Otowa, Y. Nojima, T. Miyazaki, Development of KOH activated high surface area carbon and its application to drinking water purification, Carbon 35 (1997) 1315–1319.
[30] D. Lozano-Castello, J.M. Calo, D. Cazoria-Amoros, A. Linares-Solano, Carbon activation with KOH as explored by temperature programmed techniques, and effects of hydrogen, Carbon 45 (2007) 2529–2536.
[31] M.A. Lillo-Rodenas, J. Juan-Juan, D. Cazoria-Amoros, A. Linares-Solano, About reactions occurring during chemical activation with hydroxides, Carbon 42 (2004) 1371–1375.
[32] E. Raymundo-Pinero, P. Azais, T. Cacciaguerra, D. Cazoria-Amoros, A. Linares-Solano, F. Buguin, KOH and NaOH activation mechanisms of multiwalled carbon nanotubes with different structural organisation, Carbon 43 (2005) 786–795.